Aerodynamics of Large Rotors
WP2
Deliverable 2.7
Thermal Stability

AdVanced Aerodynamic Tools for lArge Rotors

Authors: Niels Troldborg[1].

[1] **Technical University of Denmark**

Review: Gerard Schepers[2].

[2] **ECN**

Date: Nov. 2017

Agreement n.: FP7-ENERGY-2013-1/ n° 608396

Duration: November 2013 to November 2017

Coordinator: ECN Wind Energy, Petten, The Netherlands

Supported by

This project has received funding from the European Unionś Seventh Programme for research, technological development and demonstration under grant agreement No FP7-ENERGY-2013-1/ n ° 608396

1 Introduction

The loads on the AVATAR rotor operating in both a stable and unstable stratified atmospheric boundary layer over flat terrain is investigated using Large Eddy Simulations. The wind turbine rotor is modelled with the actuator line method while the flow conditions in the two cases are extracts of a full diurnal cycle. The objective of the work is to study the influence of atmospheric stability on wind turbine loads. According to the description of work it is only DTU participating in the present task.

2 Inflow simulation

This section initially describes the numerical techniques and set-up used for generating the inflow for the turbine. Subsequently, it presents the characteristics of the flow and discuss some of the limitations of the used method.

2.1 Simulation set-up

The inflow conditions for the turbine is generated by running a precursor simulation of a full diurnal cycle over flat terrain.
The simulation is carried out as LES using the Navier Stokes flow solver EllipSys3D[1,2,3] with the sub grid scale model proposed by Deardorff,[4] including the limitation of the mixing length for stable stratification.
The simulation is carried out in a Cartesian grid with dimensions $(L_x, L_y, L_z) = (3600\ m, 3600\ m, 1800\ m)$, where L_x, L_y and L_z is the domain length, width and height, respectively. The number of grid cells in each direction is $(N_x, N_y, N_z) = (384, 384, 160)$. In the main part of the domain the grid cells are cubic with a side length of 10.3 m. However, in the central region defined as $1671.4\ m \leq x \leq 1928.6R$ and $1671.4\ m \leq y \leq 1928.6R$ the grid spacing in the x and y direction is 4.3 m. The reason for concentrating cells in this part of the domain is to better resolve the flow in the region where the rotor is later to be positioned. The reason that the spacing in the z-direction is not reduced correspondingly in this region is unintentional but was unfortunately first discovered after finalizing the simulations. The lower boundary is a wall, where the wall stress and heat flux is determined from Monin-Obukhov theory using the parametrization proposed by Businger et al.[5] Symmetry conditions are applied at the upper boundary, while cyclic conditions are applied on all vertical boundaries.
The boundary conditions for the diurnal cycle are the same as in the GABLSII inter-comparison set-up.[6] This set-up assumes a constant geostrophic wind of $U_g = 3m/s$ and $V_g = 9m/s$, a Coriolis parameter of $f_c = 8.87 \cdot 10^{-}5s^{-1}$ and a uniform roughness height of $z_0 = 0.03m$.

2.2 Results

Figure 1 shows the computed daily variation of the friction velocity u_*, wall heat flux, inverse Monin-Obukhov length scale $(1/L)$ and the temperature both at and 5 m above the ground. Also included in the plots are results from measurements presented by Svensson et al.[6] In day time the ground is warmer than the air above and the ABL is unstable, whereas the opposite is true during night. As a consequence the heat flux and L are negative during day and positive during night. The computed friction velocity and heat flux is

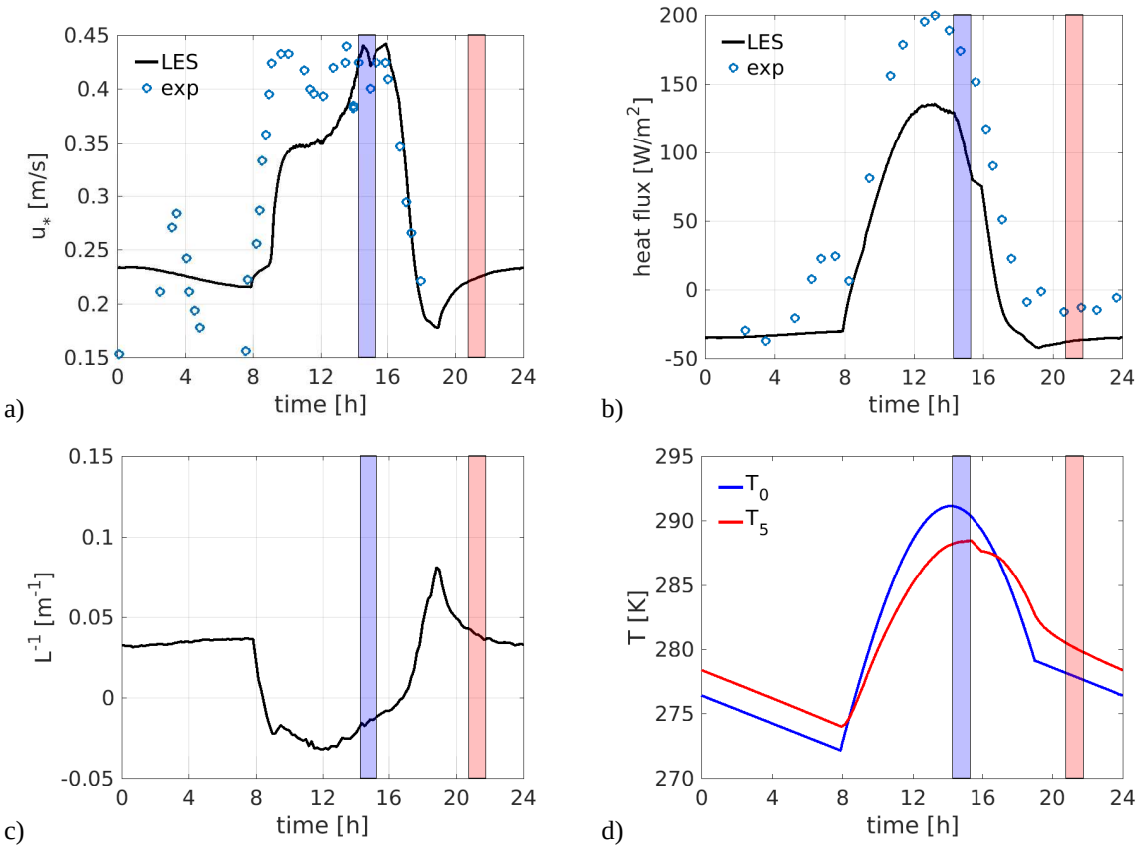

Figure 1: Friction velocity (a), wall heat flux (b), inverse Monin-Obukhov length (c) and temperature at and 5 m above the ground (d) as a function of time of day. The two periods used as inflow to the turbine are indicated as blue and red shaded regions.

seen to deviate significantly from the measurements but are on the other hand found to agree well with LES presented in the same work (not shown here) from where the measurements are taken. The deviation is most likely a result of too poor grid resolution and too simple boundary conditions but also due to uncertainties in the measurements. Neutral conditions are seen to occur only as a short transitional phase between stable and unstable conditions. From the full diurnal cycle two 1 hour periods are used as input to the simulations with a turbine included. The two periods are marked with a blue and red shaded boxes in the the plots. These periods are chosen because they represent very unstable and very stable conditions, respectively.

Figure 2 shows the horizontally averaged flow conditions near the beginning and end of each period. As seen the flow is not perfectly stationary in the selected time periods and especially in the unsteady case the velocity variance is changing significantly. However, the atmospheric boundary layer is never in balance and therefore it is not possible to get stationary periods that are also long enough to make statistics on turbine loads. Nevertheless, the velocity is not changing dramatically in the height range covered by the rotor, which is why these periods were found suitable for studying the influence of stability on wind turbine loads.

In the stable case the vertical shear is significantly larger than in the unstable case. Furthermore, the mean velocity profiles show that there is hardly any veer in the unstable case whereas a strong veer exist in the stable case. The wind direction at hub height is however nearly the same in the two cases.

Figure 3 shows the spectral characteristics of each velocity component at hub height, i.e. 132.7 m above ground for the two cases. The -5/3 slope which is characteristic of the inertial sub-range is also shown in the

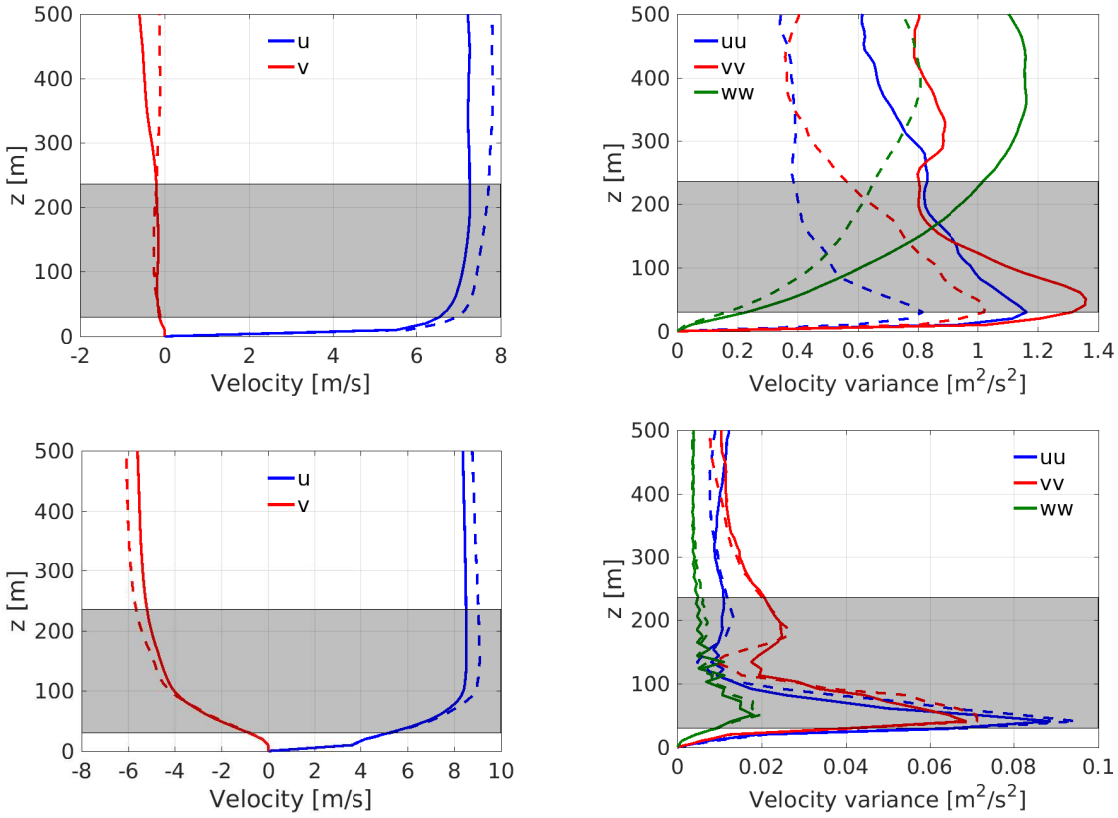

Figure 2: Horizontally averaged velocity mean and variance profiles in the selected unstable (top) and stable case (bottom). The full and dashed lines represent the results in the beginning and end of each period, respectively. The shaded region marks the region covered by the rotor

plot.
In the unstable case the inertial sub-range seems to be captured for nearly a decade of wave numbers.
In the stable case the energy is clearly much lower than in the unstable case. It is evident that the inertial sub-range is not captured in this case because the turbulence scales are small and therefore the rather coarse grid resolution does not allow resolving the inertial sub-range.

3 Wind turbine load simulations

In this section we simulate the blade loads of the AVATAR wind turbine operating in an unstable and stable atmospheric boundary layer, respectively.

3.1 Simulation set-up

The study is carried out by restarting the simulation described above at the two selected time periods but with a rotor inserted in the center of the domain at a height of 132.7 m. The rotor is modelled with the actuator line technique.[7] The influence of tower and nacelle is omitted. The blades are assumed completely stiff so this work only considers aerodynamic loads on the blades. The simulations do not include wind turbine control

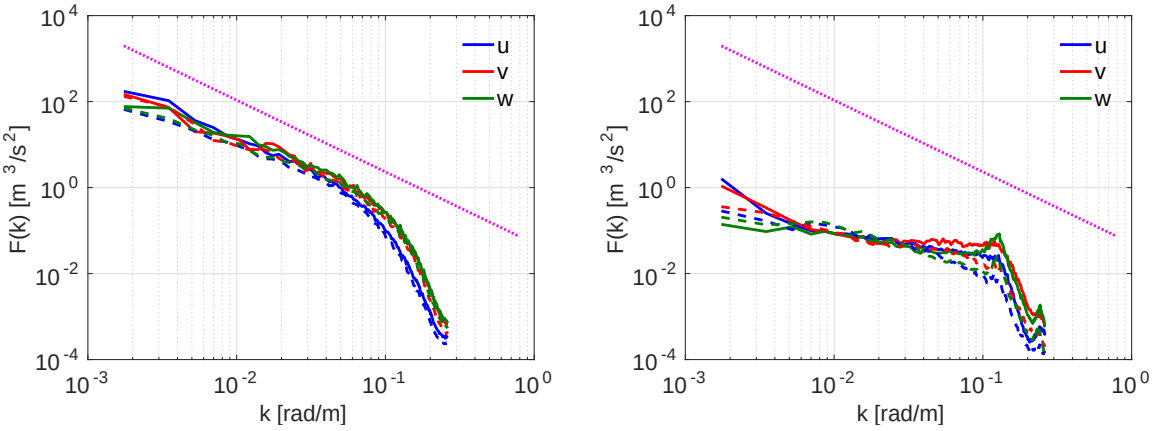

Figure 3: Spectra of velocity in coordinates aligned with the wind at hub height in the unstable (left) and stable (right) case. The full and dashed lines represent the results in the beginning and end of each period, respectively.

so yaw, rotational speed and pitch are kept constant throughout each simulation. The rotational speed is 6.3 and 8.6 RPM in the unstable and stable case respectively, while the pitch is zero. Assuming constant yaw is justified because the wind direction is not changing much during the selected time periods (see Figure 2) so the rotor is simply aligned with the mean wind direction at hub height. The assumption of constant pitch is also reasonable because the turbine operate below the rated wind speed of 10.5 m/s in the two cases. On the other hand the use of constant rotational speed is a crude assumption but since it applies equally in the two cases it should be okay when studying the influence of stability on the loads. The use of periodic boundary conditions is not a problem in the selected cases because the domain is large and because the wind direction is about 37^o which means that the wake is completely dissipated before it intersects the turbine again. This is clearly seen from the visualizations of the flow field in Figure 4.

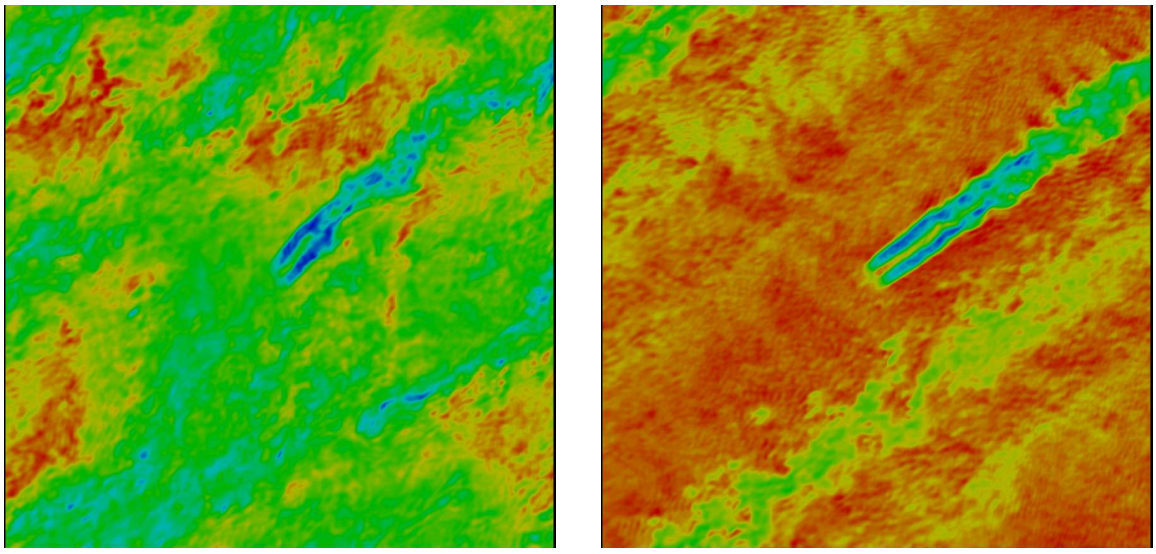

Figure 4: Snapshot of horizontal wind speed in a horizontal plane through hub height. Left) Unstable; Right) Stable

3.2 Results

Figure 5 shows the mean and standard deviation of the blade loads in the two cases. The loads are scaled with

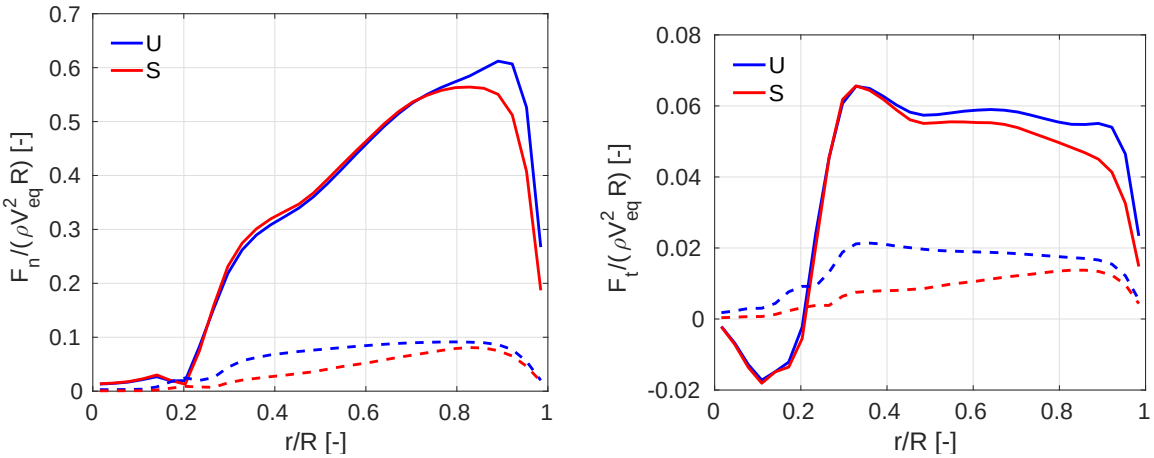

Figure 5: Normal (right) and tangential (left) force distribution. The standard deviation is shown as dashed lines.

the equivalent wind speed, which is the average of the free wind speed over the swept rotor area. Except near the tip, the scaled normal loads are close to each other, which is as expected because the thrust coefficient is constant below rated wind speed. On the other hand the driving force is smaller in the stable case, which is probably due to the high shear which means that the blades will operate away from optimal conditions. The standard deviation of the loads in the unstable case is primarily due to the high turbulence, whereas it is mainly due to the large shear in the stable case.

This is more clearly seen in Figure 6 which shows the loads binned on azimuth angle. In the stable case the loads show significant variation during a revolution but the standard deviation at each azimuth angle is significantly lower. There are some wiggles in the load distribution when the blade is at an azimuth of $\theta = 270^o$ (horizontal). The origin of these are probably caused by using a too low smearing factor in the AL force transfer function. The smearing factor was selected based on the smallest dimension of the grid cells but since the cells surrounding the turbine was accidentally not made cubic (as mentioned above) this may be the reason for the wiggles.

Figure 7 shows radial distribution of the mean and standard deviation of the flap and edgewise bending moments, respectively. Generally, the moments are greater in the unstable case, which is not surprising when comparing to Figures 5-6.

Figure 8 shows the spectrum of the flap wise root bending moment. As expected, the spectra reveal significant spikes at integer values of the rotational frequency. The overall level of the spectra is much lower in the stable case but on the other hand the spikes are far more dramatic here due to the strong shear.

Finally, Table 1 shows integral forces and standard deviation of yaw and tilt moments of the turbine in the two cases. The predicted power and thrust are found to be in rather good agreement with the operational conditions provided at the AVATAR homepage (https://www.eera-avatar.eu/do/folder?id=8740-666f6c646572). It is interesting to notice that the standard deviation of the moments are quite similar in the two cases even though there is a big difference in the turbulence level. As mentioned above this is a result of the large difference in shear.

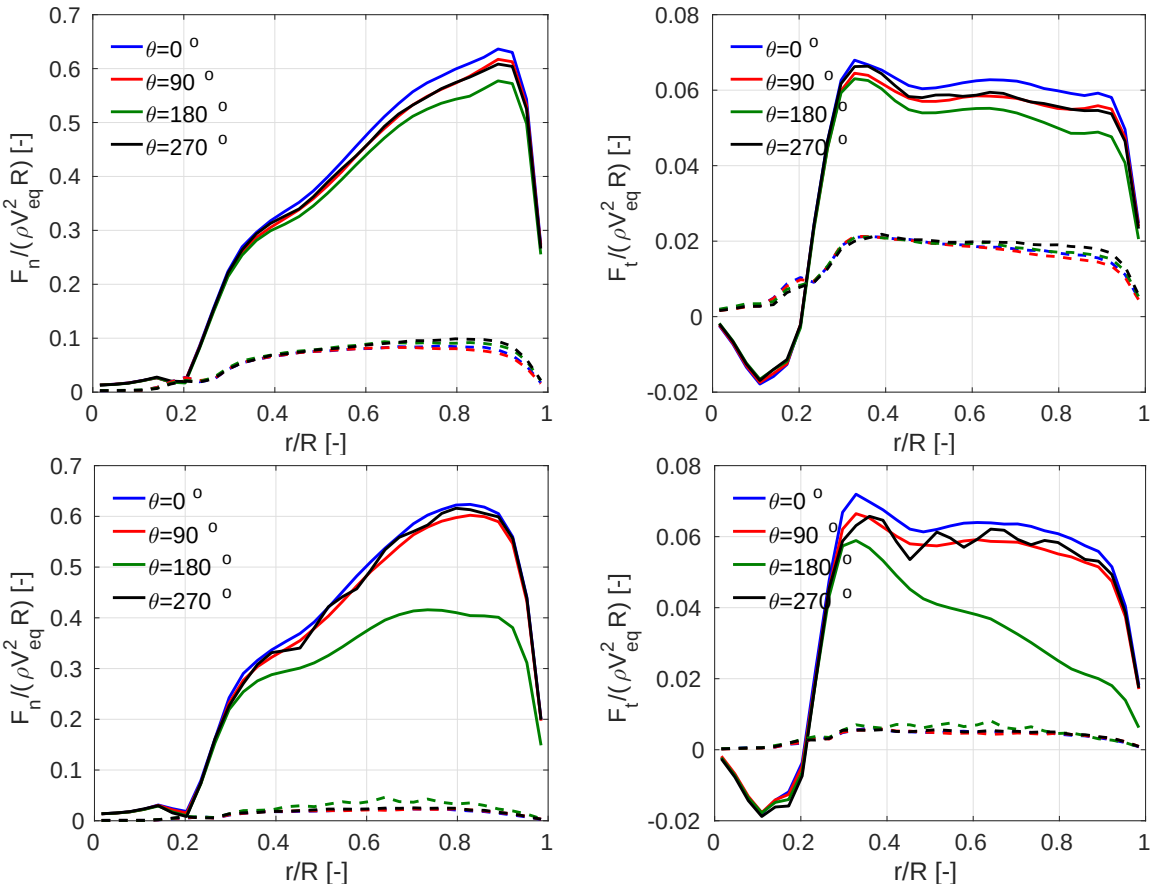

Figure 6: Normal and tangential force distribution binned on azimuth position. The blade points upwards at $\theta = 0^o$. The dashed lines show the standard deviation. Top) Unstable; Bottom) Stable.

References

[1] J.A. Michelsen. Basis3D - a platform for development of multiblock PDE solvers. Technical report AFM 92-05, Technical University of Denmark, Lyngby, 1992.

[2] J.A. Michelsen. Block structured multigrid solution of 2D and 3D elliptic PDEs. Technical Report AFM 94-06, Technical University of Denmark, 1994.

[3] N.N. Sørensen. *General Purpose Flow Solver Applied to Flow over Hills*. PhD thesis, Technical University of Denmark, 1995.

[4] J.W. Deardorff. Stratocumulus-Capped Mixed Layers Derived from a Three-Dimensional Model. *Boundary-layer Meteorology*, 18:495–527, 1980.

[5] J.A. Businger, J.C. Wyngaard, Y. Izumi, and E.F. Bradley. Flux-profile relationships in the atmospheric surface layer. *Journal of Atmospheric Sciences*, 28:181–189, 1971.

[6] G. Svensson and Coauthors. Evaluation of the Diurnal Cycle in the Atmospheric Boundary Layer Over Land as Represented by a Variety of Single-Column Models. *Boundary-layer Meteorology*, 140:177–206, 2011.

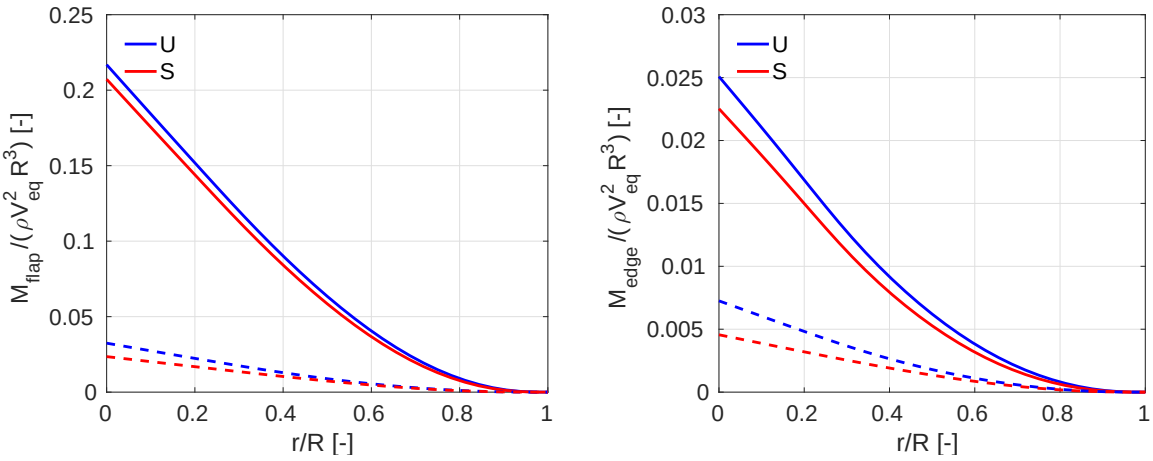

Figure 7: Flap and edgewise bending moment distribution along the blades. The standard deviation is shown as dashed lines.

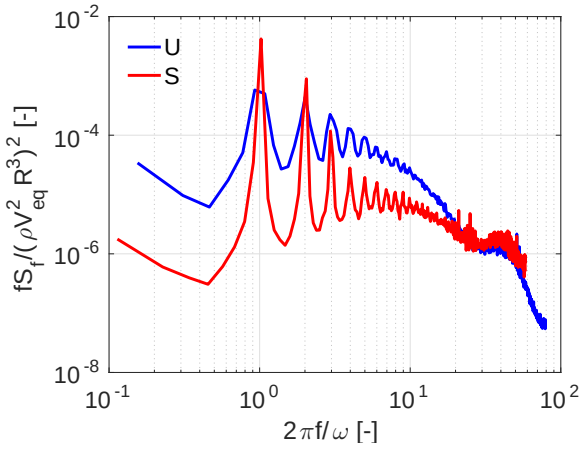

Figure 8: Spectrum of flap wise root bending moment in the two cases

[7] J.N. Sørensen and W.Z. Shen. Numerical modelling of wind turbine wakes. *Fluids Engineering*, 124:393–399, 2002.

Case	V_{eq} [m/s]	C_T [-]	C_P [-]	T [kN]	P [MW]	std_{yaw} [MNm]	std_{tilt} [MNm]
U	7.3230	0.6173	0.4397	6.7424	3.5171	1.945	1.7612
S	9.5173	0.6006	0.4136	11.0805	7.2624	1.9787	1.7766

Table 1: Statistics of integral force and moments in the two cases